Journal of Solid State Chemistry **163,** 259–266 (2002)
doi:10.1006/jssc.2001.9405, available online at http://www.idealibrary.com on IDEAL®

Cation Distribution of the Transparent Conductor and Spinel Oxide Solution $Cd_{1+x}In_{2-2x}Sn_xO_4$

D. Ko and K. R. Poeppelmeier[1]

Department of Chemistry, Northwestern University, Evanston, Illinois 60208

D. R. Kammler, G. B. Gonzalez, and T. O. Mason

Department of Materials Science and Engineering, Northwestern University, Evanston, Illinois 60208

D. L. Williamson

Department of Physics, Colorado School of Mines, Golden, Colorado 80401

and

D. L. Young and T. J. Coutts

National Renewable Energy Laboratory, Golden, Colorado 80401

Received June 13, 2001; in revised form September 14, 2001; accepted September 21, 2001

The cation distribution in the transparent conducting oxide $Cd_{1+x}In_{2-2x}Sn_xO_4$ was investigated to determine if there is a correlation between structure and electronic properties. Combined Rietveld refinements of neutron and X-ray diffraction data and ^{119}Sn Mössbauer spectroscopic analysis were used to show that the cation distribution changed with x ($0 \leq x \leq 0.7$) from a primarily normal spinel ($x=0$) to an increasingly random spinel. $CdIn_2O_4$ quenched from 1175°C has an inversion parameter of 0.31 (i.e., $(Cd_{0.69}In_{0.31})^{tet}(In_{1.69}Cd_{0.31})^{oct}O_4$). The inversion parameter decreases to 0.27 as the quench temperature is lowered from 1175°C to 1000°C. The decrease in inversion parameter with temperature correlates with an increase in optical gap from 3.0 eV to 3.3 eV for specimens prepared at 1175°C and 800°C, respectively. We show that this is a consequence of an increase in the fundamental band gap.

INTRODUCTION

Transparent conducting oxides (TCOs) are a unique class of materials that are optically transparent and electrically conducting with a wide variety of optoelectronic applications such as transparent electrodes in flat panel displays, photovoltaic cells, electrochromic devices, and transparent semiconducting devices (1). One common TCO is tin-doped indium oxide (ITO), owing to its good conductivity (~5000 S/cm) and high optical transparency between 85–90% (2). As the demand for thinner and higher performance devices increases, future TCOs will need to have higher conductivities while maintaining good optical transparency. High conductivities must be achieved by increasing the carrier mobility rather than the carrier density, because increasing carrier density results in higher free carrier absorption, thus deteriorating transparency (3). Reports of conductivities up to 8300 S/cm (4) and a large optical gap of 3.7 eV in cubic spinel Cd_2SnO_4 films (5) and comparable properties of $CdIn_2O_4$ (4) have drawn attention to these materials as possible future alternatives to ITO.

The spinel has space group $Fd\bar{3}m$, cations at the special positions 8*a* (tetrahedral coordination) and 16*d* (octahedral coordination), and oxygen anions that occupy the general positions 32*e* (6). One intriguing feature of the spinel structure is its structural and electronic flexibility, capable of incorporating a wide range of cations of different size and valence in both of the very dissimilar tetrahedral and octahedral sites in the structure. The wide range of cation distributions determined experimentally and predicted theoretically in various spinels have been shown to be intimately related to their electronic and magnetic properties (7).

In a normal spinel, the single *A* cation occupies the tetrahedral site and the two *B* cations the two equivalent octahedral sites. In an inverse spinel, one *B* cation occupies the tetrahedral site and the other *B* cation and one *A* cation

[1] To whom correspondence should be addressed.

0022-4596/02 $35.00

randomly occupy the two octahedral sites. In the completely random distribution, a statistically averaged occupation occurs in each site, i.e., $(A_{1/3}B_{2/3})^{tet}(A_{2/3}B_{4/3})^{oct}O_4$. The cation distribution is conveniently characterized by specifying the inversion parameter, δ, the fraction of tetrahedral sites occupied by B cations, i.e., $(A_{1-\delta}B_{\delta})^{tet}(A_{\delta}B_{2-\delta})^{oct}O_4$. The parameter δ equals 0, $\frac{2}{3}$, and 1 for normal, random, and inverse spinel, respectively.

The same parameter scheme can be extended to describe the cation distribution of selected ternary cation spinels, such as $A_{1+x}B_{2-2x}C_xO_4$ (A^{2+}, B^{3+}, C^{4+}), where the third cation C is a tetravalent cation with a strong tendency for octahedral occupation (Sn^{4+} or Ti^{4+}). In such systems, the cation distribution parameter δ can be defined in the same way as the inversion parameter above, i.e., the fraction of tetrahedral sites (8*a*) occupied by B cations. In the present work, the cation arrangement of the $Cd_{1+x}In_{2-2x}Sn_xO_4$ solution is successfully analyzed with this distribution scheme.

In spinels, the oxygen anions often are displaced along a [111] direction and thus an oxygen position parameter must be specified to completely define the structure. The oxygen position parameter, u, varies between 0.24 and 0.275 (origin at center of symmetry), over which the octahedral site has site symmetry $\bar{3}m$, except for $u = 0.25$ when it has cubic site symmetry $m3m$ (8).

We previously investigated the spinel solution, $Cd_{1+x}In_{2-2x}Sn_xO_4$, and reported that the electrical conductivity and optical band gap vary from 2000 S/cm at $x = 0$ to 3500 S/cm at $x = 0.70$ and from 3.0 eV at $x = 0$ to 2.8 eV at $x = 0.70$, respectively (10). That is, both properties exhibited marked changes, which was thought to reflect a possible change in the cation distribution. First-principles band structure calculations by Wei and Zhang (9) have shown that normal $CdIn_2O_4$ has a fundamental band gap 1.07 eV larger than that of inverse $CdIn_2O_4$, while inverse Cd_2SnO_4 has a band gap 0.14 eV larger than that of normal Cd_2SnO_4. Thus, in principle, the band gap can be controlled by controlling the inversion parameter. This provides an opportunity for band gap engineering to tailor these materials for specific optical and electrical applications.

Both experimental and theoretical attempts have been made to determine the cation distribution of $CdIn_2O_4$ and Cd_2SnO_4 spinels. Skribljak *et al.* (11) were unable to determine the cation distribution in spinel $CdIn_2O_4$ from XRD, but concluded that the distribution was likely to be inverse, based on the site preference enthalpies of Cd^{2+} and In^{3+} as calculated by Miller (12). In contrast to this, Shannon *et al.* (13) calculated the tetrahedral cation–oxygen bond length and the octahedral cation–oxygen bond length from the X-ray data of Skribljak *et al.* (11) and found that they most closely match the normal spinel model calculated from Shannon's radii of $^{IV}Cd^{2+}$, $^{VI}Cd^{2+}$, $^{IV}In^{3+}$, $^{VI}In^{3+}$, and $^{IV}O^{2-}$ ions (14). ^{119}Sn Mössbauer studies on thin films of Cd_2SnO_4 (5, 15) suggest that Cd_2SnO_4 spinel has a strong inverse distribution, based on clear evidence of octahedral occupation of Sn, but the distribution is somewhat uncertain in bulk Cd_2SnO_4 (16). First-principles band structure calculations by Wei and Zhang (9) indicated that $CdIn_2O_4$ should have a normal distribution, whereas Cd_2SnO_4 should have an inverse distribution. The cation distributions of $Cd_{1+x}In_{2-2x}Sn_xO_4$ ($x = 0, 0.1, 0.4$, and 0.7) have been recently studied by Brewer *et al.* (17) using atom location by channeling enhanced microanalysis (ALCHEMI). ALCHEMI revealed that $CdIn_2O_4$ was a normal spinel and the cation distribution became more random as x increased (17). Although ALCHEMI provides useful qualitative information about the distribution, it does not give a quantitative assignment.

The cations Cd^{2+}, In^{3+}, and Sn^{4+} are isoelectronic (atomic numbers of 48, 49, and 50, respectively). Consequently, their X-ray scattering factors are almost identical (18). Therefore, determining the cation distribution through conventional X-ray diffraction is impossible. Neutron diffraction, however, offers better contrast in scattering cross section between these cations and yields a more accurate estimate of the oxygen parameter, u, which is known to be sensitive to the cation distribution (8, 19, 20). Therefore, combined Rietveld refinements using time-of-flight (TOF) neutron diffraction and X-ray diffraction data were conducted in order to obtain a complete crystallographic solution to the structure.

In this paper we present the experimentally determined cation distribution of the solid solution, $Cd_{1+x}In_{2-2x}Sn_xO_4$, which we have fitted using the model of O'Neill and Navrotsky (19). This model can be used to predict the distribution for all x and at temperatures other than the quench temperature of 1175°C. In addition we demonstrate how to control the distribution in $CdIn_2O_4$ by preparing a specimen at a lower temperature (800°C) with a substantially different cation distribution by a sol–gel technique.

EXPERIMENTAL

Bulk samples of $Cd_{1+x}In_{2-2x}Sn_xO_4$ ($x = 0$, 0.50, 0.70) were prepared by mixing CdO or ^{112}CdO, In_2O_3, and SnO_2 (> 99.99% purity on cation basis, Aldrich Chemical Co., Inc.; ^{112}Cd from Trace Sciences International, Ontario, Canada) in an agate mortar and pestle under acetone, pressing $\frac{1}{4}$-in. pellets at 150 MPa, firing initially at 1000°C for 24 hours, and one or two times at 1175°C for 24 hours with intermediate grindings. Pellets were quenched in ambient air after final annealing. All specimens were fired in a cylindrical crucible with a tightly fitting lid to minimize volatilization of cadmium. Repeated grinding and firing cycles were continued until phase purity was established via powder X-ray diffraction. More details of sample preparation can be found elsewhere (10). Some $^{112}CdIn_2O_4$ samples ($x = 0$)

TABLE 1
The Neutron and X-Ray Scattering Characteristics (18) of the Atoms Involved in the $Cd_{1+x}In_{2-2x}Sn_xO_4$ Solid Solution[a]

	Z	A	C (%)	σ_c (neutron)	σ_a (neutron)	σ (X-ray)
Cd	48	—	—	3.3	2.5×10^{3}	4.2×10^{4}
^{113}Cd	48	113	12.2	12.2	2.1×10^{4}	—
^{112}Cd	48	112	24.1	6.9	2.2×10^{0}	—
In	49	—	—	2.1	1.9×10^{2}	4.5×10^{4}
Sn	50	—	—	4.9	6.3×10^{-1}	4.9×10^{4}
O	8	—	—	4.2	1.9×10^{-4}	3.0×10^{2}

[a] Z, atomic number; A, mass number; C (%), natural abundance; σ_c, neutron coherent scattering cross section (barns); σ_a, neutron absorption cross section (barns) for 2200 ms^{-1}; σ, X-ray scattering cross section for Cu $K\alpha$ (barns/atom); 1 barn = 100 fm^2.

were additionally equilibrated at 1000°C and quenched, or slowly cooled from 1175°C at the rate of 25°C/hour. One $CdIn_2O_4$ sample was prepared by a nitrate sol–gel synthesis for optical band gap measurements. First, stoichiometric amounts of CdO and In_2O_3 powders were completely dissolved into 5 N HNO_3 solution, and then the solution was slowly dried at 80°C until gel fragments formed and further dried at 150°C, and finally the obtained dry gel was calcined at 800°C to form the target oxide. All samples were shown to be single-phase spinel by X-ray diffraction.

The X-ray and neutron scattering characteristics of all the involved ions are summarized in Table 1. The neutron scattering cross sections of ^{112}Cd, In, and Sn are 6.9, 2.1, and 4.9 barns, respectively (18). Thus, the neutron scattering contrast between the cations is sufficient to determine their site occupancies, while their X-ray scattering cross sections are practically indistinguishable from each other. All diffraction samples were made using ^{112}Cd isotope because of the unacceptably large absorption cross section of the ^{113}Cd isotope (12% of naturally occurring Cd). The absorption cross section of ^{112}Cd isotope is 4 orders of magnitude smaller than that of ^{113}Cd (2.2 vs 20,600 barns for 2200 ms^{-1}, see Table 1) (18).

Time-of-flight neutron diffraction data were collected on the Special Environment Powder Diffractometer (SEPD) at the Intense Pulsed Neutron Source (IPNS) at Argonne National Laboratory. The diffractometer is described in detail by Jorgensen *et al.* (21). A fixed scattering geometry and relatively high flux at the detector, with low background, characterize this instrument, which allows rapid data collection on a small amount of sample. Neutron diffraction patterns were collected for a range of flight times corresponding to d-spacings between 0.4 and 4.0 Å, with the detectors at 144.8°, 90°, and 60°. About 1 g of sample powder was contained in a cylindrically shaped vanadium vessel for data collection. To run such a small sample, a cadmium shield was used to mask the empty part of the vanadium can, to lower the background. X-ray diffraction data were collected on a Scintag XDS 2000 diffractometer using Cu$K\alpha$ radiation. Diffraction angle (2θ) was scanned between 10° and 140° at 0.02° increments, with a 10-second collection time at each step.

The combined Rietveld refinement of neutron and X-ray data allows an unambiguous determination of the site occupancies of the three cations (^{112}Cd, In, Sn) over the crystallographically distinct spinel sites (8*a*, 16*d*). During the refinement, the occupancy factors for all elements and atom sites were constrained so as to reproduce the nominal composition of the compound and full occupancy of all atom sites.

For this analysis, the Generalized Structure Analysis System (GSAS) software (Larson and Von Dreele, 1994) was employed (22). The backgrounds for the neutron diffraction patterns were modeled using the 8–10th order polynomial function,

$$I_b = \sum_{j=1}^{N} B_j \frac{Q^{2(j-1)}}{(j-1)!}, \qquad [1]$$

where $Q = 2\pi/d$ and d is interplanar spacing. The backgrounds for the X-ray diffraction patterns were fitted with the 6–8th order cosine Fourier series function,

$$I_b = B_1 + \sum_{j=2}^{N} B_j \cos[2\theta(j-1)]. \qquad [2]$$

The absorption for neutron diffraction was corrected using the simple linear absorption function,

$$A_h = \exp(-\lambda A_B), \qquad [3]$$

where λ is wavelength and A_B is a refinable coefficient. The profile fitting for the neutron data was carried out using an exponential pseudo-Voigt convolution function (23). The profile of the X-ray spectra was modeled using a multiterm Simpson's rule integration of the pseudo-Voigt function (24). The crystallographic variables refined were the lattice parameter, the coordinate of the oxygen atom, the occupancies of the tetrahedral site (8*a*) and the octahedral site (16*d*), and the isotropic temperature factors.

Mössbauer spectra were acquired in the constant acceleration mode with both source and absorber (the sample) at room temperature. A 2-mCi $CaSnO_3$:^{119m}Sn source was used. The transmission spectra were acquired with a xenon-filled proportional counter and a 50-mm Pd foil to filter the Sn X-rays from the ^{119m}Sn γ-rays. All isomer shifts are reported relative to $CaSnO_3$. The spectra were best fitted (χ^2 close to unity) with a single quadrupole doublet with equal line widths and intensities for the pair of lines. Alternate fits that included additional single lines and quadrupole doublets did not result in improved fits. Further details of the measurements can be found elsewhere (25).

Diffuse reflectance was measured from 200 to 800 nm using a double-beam spectrophotometer with an integrating

sphere (Cary 1E with Cary $\frac{1}{3}$ attachment, Varian, Walnut Creek, CA). Baseline spectra were collected using pressed polytetrafluoroethylene (PTFE) powder compacts (Varian, part number 04-101439-00) placed in the sample and reference beams. Data were collected with a scan rate of 600 nm/min, a data interval of 1 nm, an averaging time of 0.1 second, and a signal band width of 3 nm. Pellets were mounted on a blackened sample mask. Diffuse reflectance measurements on bulk samples are analogous to transmission measurements on thin films (26). The absorption edge determined from diffuse reflectance was used to estimate an optical band gap.

RESULTS AND DISCUSSION

Combined refinements of neutron and X-ray diffraction data were conducted on four samples: $^{112}CdIn_2O_4$ quenched from 1175°C; $^{112}CdIn_2O_4$ quenched from 1000°C; $^{112}CdIn_2O_4$ slowly cooled from 1175°C; and $^{112}Cd_{1.7}In_{0.6}Sn_{0.7}O_4$ quenched from 1175°C. Parts of the

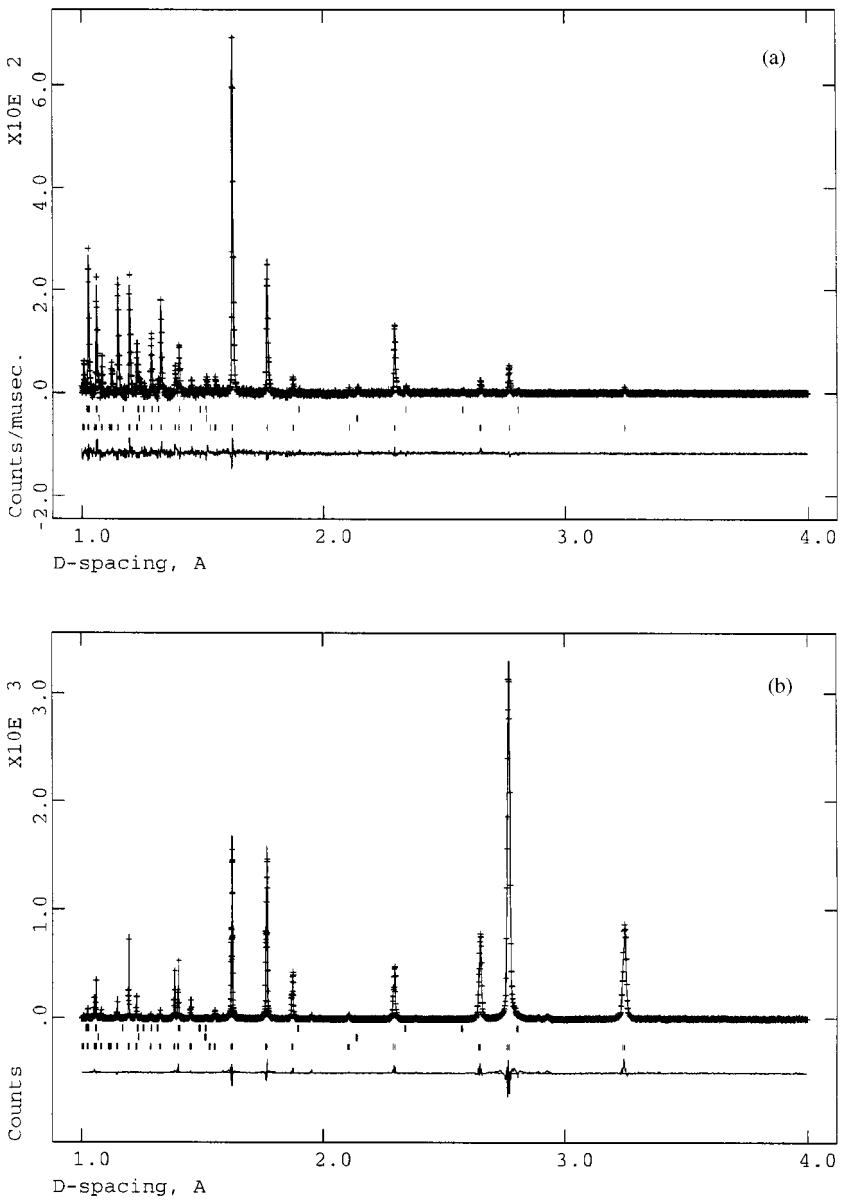

FIG. 1. Part of the neutron and X-ray diffraction data for $^{112}Cd_{1.7}In_{0.6}Sn_{0.7}O_4$. Data shown by plus marks in (a) represent data collected on the + 144.8° detector bank of the SEPD diffractometer at the IPNS in Argonne National Laboratory and in (b) represent data taken on a Scintag XDS 2000 X-ray diffractometer with Cu $K\alpha$ radiation. The solid lines are the best fit to the data from the combined refinement. Tic marks show the positions for the allowed reflections. Elemental Cd (from Cd shield) and V (V sample holder) are observed. The lower curves represent the difference between the observed and calculated profiles.

TABLE 2
The Structural Parameters of $^{112}Cd_{1+x}In_{2-2x}Sn_xO_4$ with $x=0$ for the Samples Quenched from 1175°C, Quenched from 1000°C, and Slow-Cooled at the Rate of 25°C/hour from 1175°C

$^{112}CdIn_2O_4$, Space group: $Fd\bar{3}m$ (#227)

Processing condition	1175°C	1000°C	Slow-cooled
Lattice parameter a (Å)	9.1651(1)	9.1658(1)	9.1644(1)
Inversion parameter δ[a]	0.31(1)	0.27(1)	0.26(1)
Oxygen parameter u	0.2628(1)	0.2625(1)	0.2628(1)
$100\times {}^{tet}U_{iso}$ (Å)	1.191(13)	1.062(12)	1.143(22)
$100\times {}^{oct}U_{iso}$ (Å)	1.061(15)	1.951(15)	0.925(19)
$100\times {}^{oxy}U_{iso}$ (Å)	0.554(4)	0.709(7)	0.735(13)
Tet–O bond (Å)	2.187(0)	2.183(0)	2.187(1)
Oct–O bond (Å)	2.181(0)	2.183(0)	2.180(0)
R_{wp} (%) for ND/XRD[b]	7.92/9.31	8.47/10.8	6.66/8.56
R_p (%) for ND/XRD[c]	4.72/5.28	4.86/5.88	4.10/4.78
χ^{2d}	1.30	1.59	1.39

[a] Inversion parameter δ: the occupation of In^{3+} in the tetrahedral site, i.e., $(^{112}Cd_{1-\delta}In_\delta)^{tet}(In_{2-\delta}{}^{112}Cd_\delta)^{oct}O_4$. [b] $R_{wp}=100\times\sqrt{\left(\frac{\sum w(Y_{obs}-Y_{calc})^2}{\sum wY_{obs}^2}\right)}$. [c] $R_p=100\times\left(\frac{\sum|Y_{obs}-Y_{calc}|}{\sum Y_{obs}}\right)$. [d] $\chi^2=\frac{\sum w(Y_{obs}-Y_{calc})^2}{N-P}$, where w is a statistical weight; Y_{obs}, the observed intensity; Y_{calc}, the calculated intensity; N, the number of Y_{obs}; P, the number of parameters refined.

neutron and X-ray diffraction patterns of $^{112}Cd_{1.7}In_{0.6}Sn_{0.7}O_4$ representative of all four refinements are shown together with the fits from the refinement in Fig. 1. Plus (+) marks represent data collected on either the neutron or X-ray diffractometer. Tic marks show the positions for the allowed reflections. In addition to the spinel phase (bottom), the reflections of elemental Cd (from Cd shield) and V (from V sample holder) phases were observed (top and middle, respectively) and removed from the refinement of the spinel structure by the Le Bail extraction method (27). The difference in the relative scattering factors for the neutron and X-ray experiments, as well as the good agreements between the observed profiles and the calculated profiles, are clearly shown in the figure.

The structural parameters refined for the three end member spinels at $x=0$ ($^{112}CdIn_2O_4$) described above are summarized in Table 2. The essential feature of this investigation is to understand the structural response of $CdIn_2O_4$ to temperature. Specifically, the exchange of metal cations between tetrahedral and octahedral sites as a function of temperature is of particular interest in this study. The cation distribution is represented by the inversion parameter δ, the occupancy of In^{3+} on the tetrahedral site, as in $(Cd_{1-\delta}In_\delta)^{tet}(In_{2-\delta}Cd_\delta)^{oct}O_4$. The inversion parameter δ is displayed as a function of sample thermal history in Fig. 2. It is clear from Fig. 2 that, while $CdIn_2O_4$ ($x=0$) with $\delta=0.31$ at 1175°C is closer to normal ($\delta=0$) than inverse ($\delta=1$) or random ($\delta=0.66$), there is a substantial amount

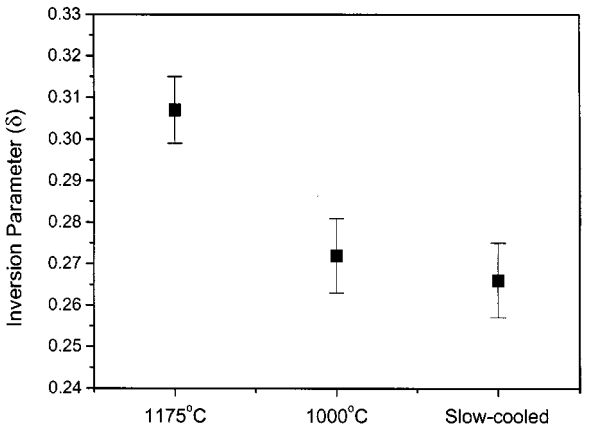

FIG. 2. Inversion parameter δ as a function of annealing temperature. Two samples were quenched from 1175°C and 1000°C, respectively. The other sample was slow-cooled from 1175°C at the rate of 25°C/hour.

of cation disordering in the structure. The degree of inversion decreases as the annealing temperature decreases from 1175°C to 1000°C. However, no noticeable change in δ was observed, within experimental error, after 1000°C with slow cooling. Therefore, the rearrangement of ^{112}Cd and In between the tetrahedral and octahedral sites (a thermally activated process) appears to freeze below 1000°C. Similar behavior has been observed in a number of previous *in situ* or *ex situ* studies of other spinel or analogous systems undergoing cation ordering (20, 28).

According to the first-principles band structure calculations by Wei and Zhang (9), the fundamental band gap for normal $CdIn_2O_4$ should be substantially larger than the one

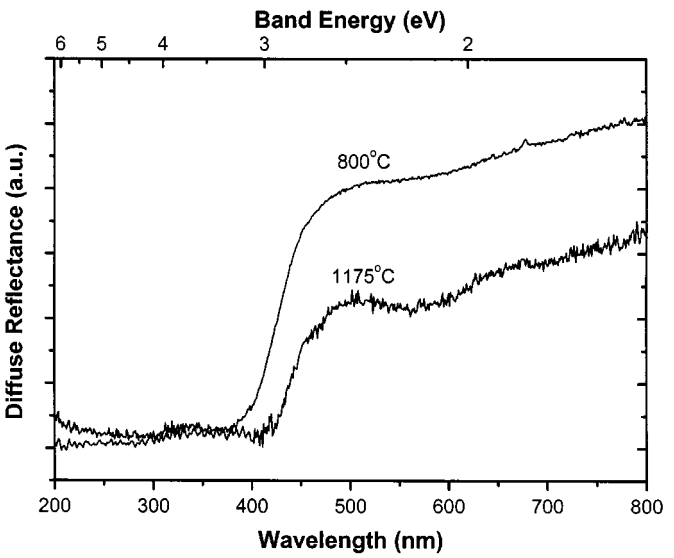

FIG. 3. Comparison of diffuse reflectance data of two differently processed $CdIn_2O_4$ samples; quenched from 1175°C and nitrate sol–gel synthesized with the final calcination at 800°C. The optical band gap increases with decreasing processing temperature.

for inverse $CdIn_2O_4$, by as much as 1.07 eV. This can be qualitatively understood as arising from lower local symmetry in inverse $CdIn_2O_4$ which leads to further repulsion of energy levels within the conduction band and within the valence band, thus producing a lower band gap. The diffuse reflectance spectra for $CdIn_2O_4$ specimens prepared at 1175°C and 800°C are presented in Fig. 3. The exchange of the cation between the tetrahedral and octahedral sites is a thermally activated process and is frozen below 1000°C as shown in Fig. 2. Consequently, the 800°C equilibrated sample was prepared by a nitrate sol–gel synthesis technique. Both samples were reduced at 400°C in a forming gas (4% H_2/balance N_2) anneal. The thermopower values at room temperature were measured to be $-53.37\ \mu V/K$ and $-36.87\ \mu V/K$ for 800°C and 1175°C annealed samples, respectively. The shift of absorption edge toward shorter wavelengths is clearly seen in the figure as the equilibration temperature decreases. Given that the sol–gel specimen has a larger thermopower magnitude, and therefore a lower carrier density, the band gap increase (by ~ 0.3 eV) from 1175°C to 800°C observed in the spectra must be a result of an increase in the fundamental band gap rather than a Moss–Burstein shift (29). Since the sol–gel derived specimen was produced at a lower temperature (800°C) than the conventional solid state specimen (1175°C), we expect the cation distribution to be more normal (i.e., $\delta_{800°C} < \delta_{1175°C}$). Thus, the observed increase in fundamental band gap is consistent with the calculated increase in fundamental gap associated with a transition between inverse and normal $CdIn_2O_4$ (9).

The crystallographic results of the Rietveld refinement for the solid solution at $x = 0.7$ ($^{112}Cd_{1.7}In_{0.6}Sn_{0.7}O_4$) are compiled in Table 3. Tin appears to reside exclusively on octahedral sites. These results were confirmed by an independent ^{119}Sn Mössbauer study (25). The Mössbauer spectrum of the $x = 0.5$ sample showed measurable quadrupole splitting. Given that the tetrahedral site has cubic symmetry in spinels, and consequently no electric field gradient, this quadrupole splitting must be attributed to ^{119}Sn in octahedral coordination. Furthermore, the model fitting of the spectrum converged to no singlet component resulting from the tetrahedral occupation. The fitting, shown in Fig. 4, unambiguously assigns all Sn ions to the octahedral sites. The preference of Sn^{4+} for the octahedral site observed in this study is also consistent with the previous Mössbauer studies for Cd_2SnO_4 ($x = 1$) in the literature (5, 15).

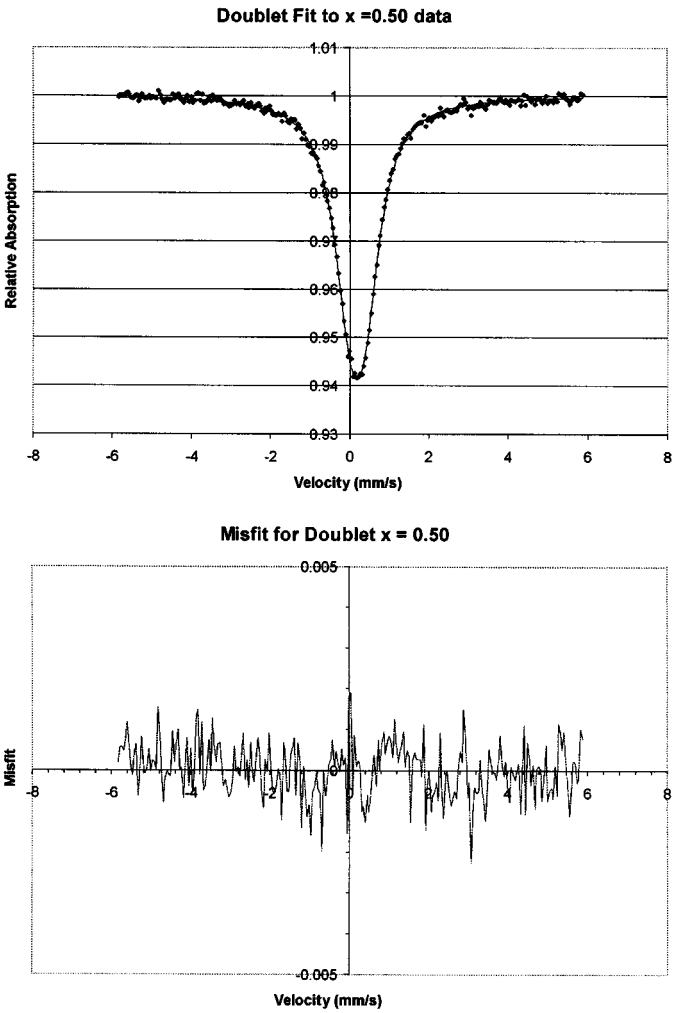

FIG. 4. ^{119}Sn Mössbauer spectra of $Cd_{1+x}In_{2-2x}Sn_xO_4$ at $x = 0.5$ are displayed with the model fitting. The refinement converged to no singlet, which indicates the occupation of 100% Sn^{4+} located solely on octahedral sites.

TABLE 3
The Structural Parameters of $^{112}Cd_{1+x}In_{2-2x}Sn_xO_4$ with x=0.7 Refined by a Combined Neutron and X-Ray Rietveld method[a]

$^{112}Cd_{1.7}In_{0.6}Sn_{0.7}O_4$, Space group: $F\,d\,\bar{3}\,m$ (#227), $a = 9.1763(1)$ Å

Atom	Site	x	y	z	$100 \times U_{iso}$ (Å^2)	Fraction
^{112}Cd	8*a*	$\frac{1}{8}$	$\frac{1}{8}$	$\frac{1}{8}$	1.042(2)	0.79(2)
In	8*a*	$\frac{1}{8}$	$\frac{1}{8}$	$\frac{1}{8}$	1.042(2)	0.23(1)
Sn	8*a*	$\frac{1}{8}$	$\frac{1}{8}$	$\frac{1}{8}$	1.042(2)	−0.02(2)
In	16*d*	$\frac{1}{2}$	$\frac{1}{2}$	$\frac{1}{2}$	0.891(2)	0.18(6)
Sn	16*d*	$\frac{1}{2}$	$\frac{1}{2}$	$\frac{1}{2}$	0.891(2)	0.36(1)
^{112}Cd	16*d*	$\frac{1}{2}$	$\frac{1}{2}$	$\frac{1}{2}$	0.891(2)	0.46(1)
O	32*e*	0.2633(1)	0.2633(1)	0.2633(1)	1.183(8)	1.0

[a] The sample was prepared by quenching from 1175°C. The residuals, R_{wp}/R_p, were 7.43/4.64% and 6.08/4.39% for neutron and X-ray data, respectively. $\chi^2 = 1.26$. Tetrahedral bond length R(tet–O): 2.198(1) Å; Octahedral bond length R(oct–O): 2.179(1) Å.

Because Sn^{4+} occupies only the octahedral site (16*d*), only one parameter is needed to completely describe the cation distribution of the solid solution, $Cd_{1+x}In_{2-2x}Sn_xO_4$ ($x > 0$). That is, the distribution parameter δ represents the fraction of the tetrahedral sites (8*a*) occupied by In^{3+}. The cation distribution for $Cd_{1+x}In_{2-2x}Sn_xO_4$ is specified

TABLE 4
Cation Distribution along the Ternary Spinel $Cd_{1+x}In_{2-2x}Sn_xO_4$

Cation	Tetrahedral occupancy	Octahedral occupancy	Sum
Cd^{2+}	$1-\delta$	$x+\delta$	$1+x$
In^{3+}	δ	$2-2x-\delta$	$2-2x$
Sn^{4+}	0	x	x
Sum	1	2	3

in Table 4. The only independent variable for a specific composition x is δ. Therefore, the cation distribution $(^{112}Cd_{0.77}In_{0.23})^{tet}(^{112}Cd_{0.93}In_{0.37}Sn_{0.7})^{oct}O_4$ for $x = 0.7$ (see Table 3) is now represented by $\delta = 0.23$. Given that the calculated fundamental band gap reduction from normal $CdIn_2O_4$ to inverse Cd_2SnO_4 is 0.8 eV (30), the band gap decrease from $CdIn_2O_4$ to $Cd_{1.7}In_{0.6}Sn_{0.7}O_4$ is linearly interpolated to be 0.56 eV. However, the optical gap can be further varied in TCOs by changing the carrier density (the well-known Moss–Burstein shift (29)). The carrier density also directly affects the overall conductivity of the TCO. As a result, the wide-range solid solution and the tunable cation distribution in $Cd_{1+x}In_{2-2x}Sn_xO_4$ provide means of changing the fundamental band gap of these materials, which yields an additional degree of freedom that is useful in optimizing these materials for specific optoelectronic applications.

In Fig. 5, the cation distributions in the system, $Cd_{1+x}In_{2-2x}Sn_xO_4$, at 1175°C are summarized. The smooth curves connecting the data are the results of a fit based on the thermodynamic model of O'Neill and Navrotsky (19). In their model the enthalpy of cation mixing for a simple AB_2O_4 spinel is given by, $\alpha\delta + \beta\delta^2$, from lattice energy where the linear coefficient, α, is the difference in site preference enthalpies for the A and B cations, and the quadratic coefficient β is a constant of -20 kJ/mol and -60 kJ/mol for 2-3 and 2-4 spinels, respectively. In general, both configurational and nonconfigurational entropy contributions (from crystal field electronic effects) to the free energy of cation mixing are also considered. Since Cd^{2+}, In^{3+}, and Sn^{4+} have closed electronic orbitals, the nonconfigurational entropy effects were ignored. In order to model the cation distribution in a ternary spinel such as $A_{1+x}B_{2-2x}C_xO_4$, it is necessary, in general, to use two separate enthalpies of mixing, α_{AB} and α_{AC}. Since, however, the Sn^{4+} is located only on octahedral sites throughout the solid solution, $Cd_{1+x}In_{2-2x}Sn_xO_4$, a single enthalpy of mixing, $\alpha_{Cd-In}\delta + \beta_{2-3}\delta^2$, is sufficient. The fitted cation distribution illustrated in Fig. 5 was plotted using the equation,

$$-RT\ln\left[\frac{\delta(x+\delta)}{(2-2x-\delta)(1-\delta)}\right] = \alpha_{Cd-In} + 2\beta(\delta + x). \quad (4)$$

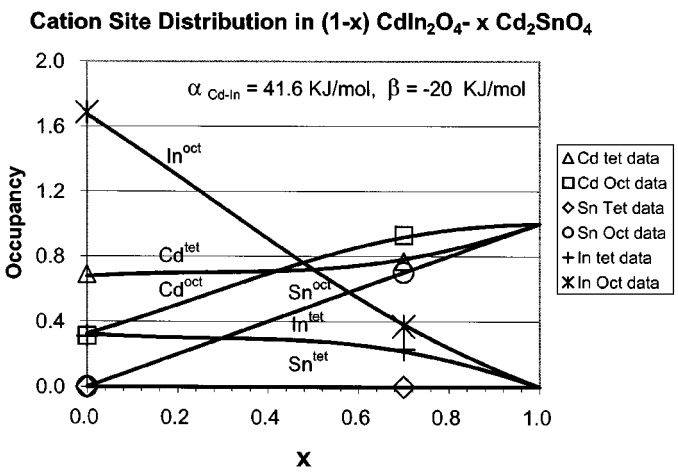

FIG. 5. Cation distribution along $Cd_{1+x}In_{2-2x}Sn_xO_4$. The data at $x = 0$ and $x = 0.7$ were fitted with the thermodynamic model of O'Neill and Navrotsky (19). The solid lines represent the distributions calculated by the model.

A value of 41.6 kJ/mol for α produced the best fit to the data in Fig. 5 with β equal to -20 kJ/mol, the constant for 2-3 spinels. It should be remembered that the fit shown in Fig. 5 is dependent on the measurements, which were conducted not *in situ*, but on samples prepared by quenching from the target annealing temperature. Furthermore, the statistical soundness is weak in this case because only two compositions were used. Despite these reservations, one key feature stands out from the model. The balance of Cd^{2+} and In^{3+} on the tetrahedral site remains nearly constant; that is, δ changes from 0.31 to 0.23 from $x = 0$ to $x = 0.7$, and essentially all the substitution takes place on the octahedral sublattice throughout the solution until near the end when there is no longer sufficient In^{3+} present to maintain the balance. At this point, the tetrahedral In^{3+} is rapidly replaced with Cd^{2+}. This area of rapid change coincides with the terminal point of the bulk spinel solid solution ($x = 0.75$) (10). Thus, it would appear that the structure becomes unstable beyond this point. Consequently, bulk compositions between $x = 0.75$ and $x = 1$ consist of a two-phase mixture of orthorhombic Cd_2SnO_4 and the terminal spinel composition $Cd_{1.75}In_{0.5}Sn_{0.75}O_4$.

CONCLUSIONS

The cation distribution of the transparent conducting oxide solution, $Cd_{1+x}In_{2-2x}Sn_xO_4$ $(0 \le x \le 0.75)$, was quantitatively characterized for the first time by a combined Rietveld refinement of TOF neutron diffraction and X-ray diffraction data and ^{119}Sn Mössbauer spectroscopic analysis.

The end member spinel, $CdIn_2O_4$, has been unambiguously determined to be a normal type spinel. However, a substantial amount of cation mixing was found, as much

as $\delta = 0.31$. The cation disordering was significantly reduced from $\delta = 0.31$ to $\delta = 0.27$ when the equilibration temperature decreased from 1175°C to 1000°C. This cation order–disorder behavior was electronically manifested by an optical band gap increase (by ~ 0.3 eV) in the diffuse reflectance measurements, which has been traced to a change in the fundamental band gap, when the equilibration temperature decreased from 1175°C to 800°C. The unique dependence of the optical gap on controllable parameters, such as the composition and cation distribution which can also be altered with temperature, provides a unique opportunity for band gap engineering of these materials for various technical applications.

The cation site occupancies of the $x = 0.7$ sample at 1175°C in the $Cd_{1+x}In_{2-2x}Sn_xO_4$ solution have been determined to be $(Cd_{0.77}In_{0.23})^{tet}(Cd_{0.93}In_{0.37}Sn_{0.7})^{oct}O_4$ (i.e., $\delta = 0.23$). It is found that Sn^{4+} ions occupy only the octahedral sites (16*d*) and the cation mixing parameter δ is 0.23. The $x = 0$ and $x = 0.70$ cation distribution data were fitted using the model of O'Neill and Navrotsky (19). The fit shows a steady decrease in the In^{3+} concentration and an increase in the Cd^{2+} concentration on the octahedral site up to $x = 0.7$, coinciding with the end of the bulk solid solution at $Cd_{1.75}In_{0.5}Sn_{0.75}O_4$, followed by saturation of the octahedral Cd^{2+} and subsequent replacement of tetrahedral In^{3+} by Cd^{2+} as x increases beyond 0.7. It appears that the spinel structure is unstable beyond this point.

ACKNOWLEDGMENTS

This work was supported in part by the MRSEC program of the National Science Foundation (DMR-0076097) at the Materials Research Center of Northwestern University and in part by the U.S. Department of Energy through the National Renewable Energy Laboratory under subcontract number AAD-9-18668-05. The central facilities of the Materials Research Center were used extensively in the research. The authors thank James D. Jorgensen and Simine M. Short for their discussion and help in performing the neutron scattering experiments. The IPNS is supported by the Department of Energy (W-31-109-ENG-38). D.R.K. was supported by a National Science Foundation graduate fellowship.

REFERENCES

1. R. G. Gordon, *MRS Bull.* **25,** 52–57 (2000); H. Kawazoe, H. Yanagi, K. Ueda, and H. Hosono, *MRS Bull.* **25,** 28–36 (2000); B. G. Lewis and D. C. Paine, *MRS Bull.* **25,** 22–27 (2000).
2. N. R. Lyman, *in* "Transparent Electronic Conductors" (M. K. Carpenter and D. A. Corrigan, Eds.), Proc. Symp. Electrochrom. Mater., Proc. Electrochem. Soc., Hollywood, FL, Electrochem. Soc. Pennington, NJ, 1989.
3. T. J. Coutts, X. Wu, W. P. Mulligan, and J. M. Webb, *J. Elec. Mater.* **25,** 935–943 (1996); W. P. Mulligan and T. J. Coutts, "Measurement of the Effective Mass of Transparent Conducting Films of Cadmium Tin Oxide" (R. Fulks, G. P. D. Slobodin, and T. Yuzuriha, Eds.), Flat Panel Display Materials III, Proc. Mater. Res. Soc. Symp., San Francisco, Mater. Res. Soc., Warrendale, PA, 1997; D. L. Young, Ph. D. Dissertation, Colorado School of Mines, 2000.
4. X. Wu, T. J. Coutts, and W. P. Mulligan, *J. Vac. Sci. Technol. A* **15,** 1057–1062 (1997).
5. W. P. Mulligan, Ph.D. Dissertation, Colorado School of Mines (1997).
6. R. W. G. Wyckoff, "Inorganic Compounds $R_x(MX_4)_4$, $R_x(M_nX_p)_y$ Hydrates and Ammoniates," 2nd Ed., Vol. 3. Wiley, New York, 1960.
7. R. J. Hill, J. R. Craig, and G. V. Gibbs, *Phys. Chem. Miner.* **4,** 317–339 (1979); A. Navrotsky and O. J. Kleppa, *J. Inorg. Nucl. Chem.* **29,** 2701–2714 (1967).
8. H. S. C. O'Neill and A. Navrotsky, *Am. Miner.* **68,** 181–194 (1983).
9. S.-H. Wei and S. B. Zhang, *Phys. Rev. B* **63,** 1–8 (2001).
10. D. R. Kammler, T. O. Mason, and K. R. Poeppelmeier, *Chem. Mater.* **12,** 1954–1960 (2000).
11. M. Skribljak, S. Dasgupta, and A. B. Biswas, *Acta Crystallogr.* **12,** 1049 (1959).
12. A. Miller, *J. Appl. Phys.* **30,** 24 (1959).
13. R. D. Shannon, J. L. Gillson, and R. J. Bouchard, *J. Phys. Chem. Solids* **38,** 877–881 (1977).
14. R. D. Shannon, *Acta. Crystallogr. A* **32,** 751–767 (1976).
15. C. M. Cardile, A. J. Koplick, R. McPherson, and B. O. West, *J. Mater. Sci. Lett.* **8,** 370–372 (1989); T. Stapinski, E. Japa, and J. Zukrowski, *Phys. Stat. Solidi A* **103,** K93 (1987).
16. C. M. Cardile, *J. Phys. Chem. Solids* **50,** 221–222 (1989).
17. L. N. Brewer, D. R. Kammler, T. O. Mason, and V. P. Dravid, *J. Appl. Phys.* **89,** 951–954 (2001).
18. A. J. C. Wilson, "International Tables for Crystallography," 1st Ed., Vol. C. Kluwer Academic Publishers, Dordrecht/Boston/London, 1995.
19. H. S. C. O'Neill and A. Navrotsky, *Am. Miner.* **69,** 733–753 (1984).
20. S. A. T. Redfern, R. J. Harrison, H. S. C. O'Neill, and D. R. R. Wood, *Am. Miner.* **84,** 299–310 (1999).
21. J. D. Jorgensen, *et al.*, *J. Appl. Crystallogr.* **22,** 321–333 (1989).
22. A. C. Larson and R. B. Von Dreele "General Structure Analysis System (GSAS)," Los Alamos National Laboratory Report LAUR 86-748. Los Alamos, NM, 1994.
23. *GSAS Manual.* Available at: ftp://ftp.lanl.gov/public/gsas/manual/GSAS manual.pdf.
24. C. J. Howard, *J. Appl. Crystallogr.* **15,** 615–620 (1982).
25. D. R. Kammler, *et al.*, *J. Appl. Phys.*, in press (2001).
26. H. G. Hecht, *in* "The Present Status of Diffuse Reflectance Theory" (W. W. Wendlandt, Ed.). Plenum Press, New York, 1968.
27. *GSAS Manual.* Available at: ftp://ftp.lanl.gov/public/gsas/manual/GSAS manual.pdf.
28. S. A. T. Redfern, C. M. B. Henderson, B. J. Wood, R. J. Harrison, and K. S. Knight, *Nature* **381,** 407–409 (1996); R. J. Harrison, S. A. T. Redfern, and H. S. C. O'Neill, *Am. Miner.* **83,** 1092–1099 (1998); S. A. T. Redfern, C. M. B. Henderson, K. S. Knight, and B. J. Wood, *Eur. J. Miner.* **9,** 287–300 (1997).
29. T. S. Moss, *Proc. Phys. Soc.* **67B,** 775–882 (1954); E. Burstein, *Phys. Rev.* **93,** 632 (1954).
30. S.-H. Wei and S. B. Zhang, personal communication, October 2000.